Solid-phase epitaxial regrowth of amorphous silicon containing helium bubbles

M. F. Beaufort,[1,a)] L. Pizzagalli,[1] A. S. Gandy,[1,3] E. Oliviero,[2] D. Eyidi,[1] and S. E. Donnelly[3]
[1]*Laboratoire de Physique des Matériaux, UMR6630, Université de Poitiers, SP2MI, Bd Marie et Pierre Curie, BP30179, 86962 Futuroscope-Chasseneuil Cedex, France*
[2]*Instituto de Física, Universidade Federal do Rio Grande do Sul, Av Bento Gonçalves 9500, Caixa Postal 15051, 91501-970 Porto Alegre, Rio Grande do Sul, Brazil*
[3]*Institute for Materials Research, University of Salford, Manchester M5 4WT, United Kingdom*

(Received 9 July 2008; accepted 15 September 2008; published online 7 November 2008)

Transmission electron microscopy has been used to study processes occurring when a layer of amorphous silicon (*a*-Si) containing helium-filled cavities buried in crystalline silicon (*c*-Si) recrystallizes by solid phase epitaxial growth (SPEG). The buried layer was formed in (100) silicon by means of bombardment with 150 keV Li ions with the bubbles resulting from subsequent implantation of 80 keV He ions; the energies being chosen to ensure that the resulting bubble distribution was entirely contained within the amorphous layer. The presence of bubbles in *a*-Si undergoing SPEG at a (100) interface with *c*-Si has previously been observed to give rise to the formation of microtwin lamellas, assumed to nucleate at the bubble surfaces; however, the present work indicates clearly that, in fact during SPEG, many microtwins nucleate remote from the bubbles. There is also an apparent interaction between the amorphous-crystalline (*a*-*c*) interface and the bubbles, in which the bubbles seem to be swept by the moving interface. The paper will discuss possible mechanisms for both phenomena, in terms of interstitial defects for the nucleation of microtwins and in terms of enhanced bubble mobility in *a*-Si for the apparent interaction between the *a*-*c* interface and the bubbles. © *2008 American Institute of Physics*. [DOI: 10.1063/1.3009383]

I. INTRODUCTION

Cavities resulting from the incorporation of inert gas ions in solids by energetic implantation or transmutation reactions in nuclear reactors have been of technical interest for many decades, largely as a result of the detrimental effects that the presence of such defects may have on the structural integrity of components of both fission reactors and proposed fusion reactors. Many studies have been devoted to cavities induced by inert gas implantation in metals.[1–4] More recently, the deliberate creation of nanocavities in semiconductors by ion implantation of gases such as helium and hydrogen has also excited considerable interest in view of the beneficial use of these defects for purposes that include the Smart Cut® process[5] (used in the fabrication of silicon-on-insulator structures) and possible proximity gettering in microelectronic devices.[6–9] These technological interests have served as a driver for researchers to develop a fundamental understanding not only of the processes giving rise to nanocavity formation but also of the behavior of other extended defects that may be formed comcomitantly with the cavities.

Earlier work on the development of helium-filled nanocavities in silicon[10] that was heavily predamaged or amorphized showed that a moving interface between heavily damaged and undamaged silicon during a high temperature anneal led to a morphology indicative of a "sweeping" of the helium and vacancies and/or small helium bubbles by the moving interface. Similar results have been obtained after neon implantation at room temperature in silicon.[11] More recent preliminary work on this topic has strengthened the view that such a sweeping effect does indeed occur at amorphous/crystalline (*a*-*c*) interfaces but has also shown that extended defects form in the recrystallized material when such cavities are present.[12]

The purpose of the present paper is to report a detailed study both of the interaction of nanocavities in silicon with moving *a*-*c* interfaces and of the formation of the microtwin lamellas (MTLs) that are observed to form when amorphous material containing such cavities recrystallizes by SPEG. Note that the word "cavity" will be used to signify both bubbles (gas filled) and voids (empty).

II. EXPERIMENTAL DETAILS

Czochralski-grown *n*-type single-crystal (100) Si wafers with a resistivity of 1–2 Ω cm were cleaved to produce samples of a few cm^2 in size. An amorphous layer was then produced in these specimens by implantation at ≈77 K with 150 keV Li ions to a fluence of 7×10^{15} Li ions/cm^2. The conditions were chosen following Rutherford backscattering measurements on Li-implanted Si, which indicated that a buried amorphous layer centered on a depth of about 600 nm would result from this treatment. Previous work has also indicated that the radiation damage in the *c*-Si close to the *a*-*c* interface could be largely removed by means of 30 min anneal of the specimen at 400 °C following the Li implantation, resulting in a sharper *a*-*c* interface.[13] Unless otherwise stated this process was adopted in the experiments reported here. A number of specimens were subsequently implanted at

[a)]Electronic mail: marie.france.beaufort@univ-poitiers.fr.

 © 2008 American Institute of Physics

Downloaded 10 Nov 2008 to 194.167.47.253. Redistribution subject to ASCE license or copyright; see http://jap.aip.org/jap/copyright.jsp

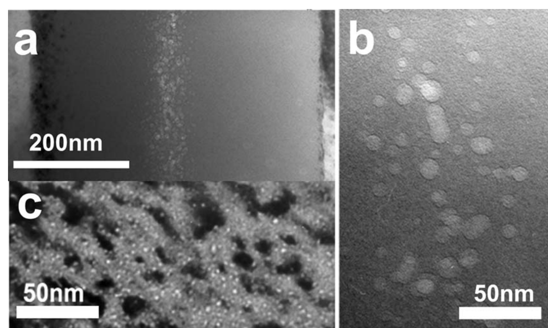

FIG. 1. ⟨110⟩ cross-sectional TEM micrographs of helium bubbles in silicon. (a) Bright-field image, taken down zone; kinematical diffraction conditions; underfocus, showing helium bubbles formed initially in a buried amorphous region in *c*-Si by implantation with 80 keV helium ions to a fluence of 2.5×10^{16} ions/cm^2 following Li implantation and 400 °C anneal for 30 min (to sharpen interfaces). (b) Higher magnification view of a part of the bubble distribution observed in Fig. 1(a), kinematical diffraction conditions, and underfocus. High pass filter was applied to enhance bubble contrast. (c) Bright-field image showing helium bubbles formed in *c*-Si under identical implantation conditions. It can be seen that the bubbles in the *c*-Si are significantly smaller than those in the *a*-Si.

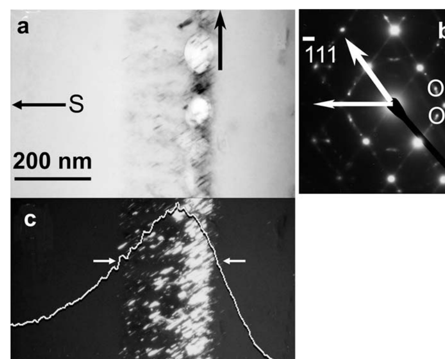

FIG. 2. ⟨110⟩ cross-sectional TEM image of helium bubbles initially in buried amorphous region in *c*-Si after a recrystallizing anneal at 600 °C. (a) Bright-field image using [111] two-beam conditions; kinematical diffraction conditions; underfocus. "S" indicates the direction of the surface. The arrow at the top of the image indicates the position of the peak in the bubble distribution prior to the anneal. (b) Dark-field TEM micrograph imaged using one of the supplementary diffractions spots (see diffraction pattern). Damage distribution calculated using the Monte Carlo code SRIM has been superimposed. (c) Selected area electron diffraction pattern from region shown in (a) and (b). Supplementary spots from microtwins are visible as a broken ring superimposed on diffraction pattern of single crystal. Two such spots indicated by white circles.

room temperature with 80 keV helium ions to a fluence of 2.5×10^{16} ions/cm^2. Calculations with the Monte Carlo code SRIM (Ref. 14) indicated that He implantation at this energy should result in a projected range of the implanted gas of 600 nm, putting it in the center of the amorphous band.

Some specimens were then annealed under vacuum at 600 °C for 30 min. All the specimens at the various stages of processing were prepared for cross-sectional transmission electron microscopy using the tripod polishing technique, followed by ion milling in a Gatan precision ion polishing system in order to achieve electron transparency. Both a JEOL 200CX TEM operating at 200 keV and a JEOL 3010 TEM operating at 300 keV were used to analyze the samples with images recorded on photographic negatives and subsequently digitized at a resolution of 1200 pixels/in. A number of specimens were also annealed *in situ* in the TEM using a double-tilt heating holder. In these cases, experiments were recorded on either digital video or analog Super-VHS tape. The video recordings were subsequently transferred to a computer for viewing and processing.

III. RESULTS AND DISCUSSION

Figure 1(a) is a cross-sectional micrograph of a specimen containing a buried amorphous layer that has been implanted with helium ions so as to form a bubble distribution in the center of the amorphous band. The image has been recorded under [110] down-zone conditions in which strong Bragg diffraction in the crystalline silicon (not present in the amorphous layer) provides contrast that serves to delineate the amorphous band. In addition, defocusing the objective lens (1000 nm underfocus) provides a Fresnel contrast that renders the bubbles visible as a light region surrounded by a dark fringe. Figure 1(b) is a higher magnification view of part of the bubble distribution where it can be seen that many of the bubbles have a somewhat irregular shape rather than spherical (circular in projection). For purposes of comparison, Fig. 1(c) presents an image of helium bubbles formed in *c*-Si under identical implantation conditions, where it can be seen that the bubbles in the *c*-Si are significantly smaller than those in the *a*-Si.

It should be noted that experiments were also carried out in which a much smaller fluence of He (5×10^{15} ions/cm^2) was implanted under otherwise the same conditions. In this case, just as in crystalline silicon, no bubbles were observed either directly after implantation or following a subsequent recrystallizing anneal. This is assumed to be due to insufficient helium being present locally to form stable bubble nuclei. Any submicroscopic helium agglomerates that form during implantation then dissociate during any subsequent anneal, with loss of helium from the specimen.

With a view to study the effects on the cavities of recrystallization of the amorphous layer and given that amorphous silicon is known to undergo solid phase epitaxial growth (SPEG) at temperatures above 550 °C,[15] portions of the specimen from which the micrograph in Fig. 1(a) was obtained were subjected to an anneal in a vacuum furnace for 30 min at 600 °C. Cross-sectional micrographs were then recorded from this material and these are shown in Fig. 2. The bright-field micrograph shown in Fig. 2(a) has been recorded under "off-Bragg" conditions, in which the specimen is tilted a few degrees away from the [110] zone axis used in Fig. 1(a) in order to better image the cavities. A small underfocus has also been employed here, as in Fig. 1, to provide clear images of the cavities, which in this case can be seen to have greatly increased in size during the recrystallization. The arrow at the top of the image indicates the position of the peak in the bubble distribution prior to the anneal (i.e., as seen in Fig. 1), and it is clear that the peak in the cavity distribution has shifted by approximately 60 nm toward the surface. Figure 2(b) presents the selected area diffraction pattern from the area shown in Fig. 2(a) in which supplementary reflections can be seen, which are not normally present for

Downloaded 10 Nov 2008 to 194.167.47.253. Redistribution subject to ASCE license or copyright; see http://jap.aip.org/jap/copyright.jsp

(110) silicon and which were not present in the specimen prior to the anneal (e.g., as indicated by white circles). Such reflections have been observed previously and are known to be associated with MTLs. These defects are frequently observed when *a*-Si undergoes SPEG at a (111) interface.[16] The image shown in Fig. 2(c) is a dark-field micrograph taken using one of these supplementary reflections. The damage distribution as calculated using the Monte Carlo code SRIM (Ref. 14) is overlayed on this image, (with an arbitrary vertical scale) from which it can be seen (horizontal arrows) that the MTLs would appear to be associated with a concentration of radiation damage above some threshold value. This will be discussed further below. For (100) SPEG MTLs are not normally observed, the exceptions being when impurities or defects are known to exist in the *a*-Si. In particular, MTLs have been previously observed following SPEG of amorphous layers containing gas bubbles[17,18] and have been attributed to nucleation on the bubbles themselves; however, the presence of many MTLs remote from the bubble distribution, as evidenced by Fig. 2, casts doubt on this interpretation.

With the aim of elucidating the mechanism of MTL formation and the processes giving rise to the observed displaced cavity distribution, two *in situ* experiments were carried out in which bright-field TEM images were continuously recorded on videotape and later analyzed, following transfer to a computer. Videoclips from these recordings are available and can be downloaded or webstreamed.[19]

Before discussing the *in situ* observations, it is important to note that there are important differences between anneals carried out on bulk specimens and those carried out on the thin foils prepared for cross-sectional TEM studies. In a bulk specimen, there is only one surface in close proximity to the buried amorphous layer and that surface is parallel to the *a*-*c* interfaces. In the case of the thin foil, however, there are two additional surfaces and these both intersect the *a*-*c* interfaces at right angles. A major consequence of this is that, in the *in situ* experiments, defects can be lost to surfaces that do not exist in the bulk case. For instance, where bubble motion occurs and where that bubble motion, in the bulk case, is confined to the *a*-Si layer, the observed morphology at the end of the anneal may consist of cavities still entirely confined to the region of the specimen originally occupied by the amorphous layer. In the *in situ* anneal, however, cavity motion in a direction parallel to the a-c interface may result in the loss of cavities at a surface. In addition, at temperatures where defects are being thermally created at surfaces, the presence of the two additional surfaces may increase significantly the concentration of such defects within the specimen. Finally, stress relief parallel to the *a*-*c* interfaces, which would not occur in the bulk material, can occur in the thin foil and this may also modify the final morphology of the specimen.

A. Microtwin formation

Turning first to the *in situ* observations of MTL formation, it is clear from the video recordings of the *in situ* experiments that the two *a*-*c* interfaces do not start moving at

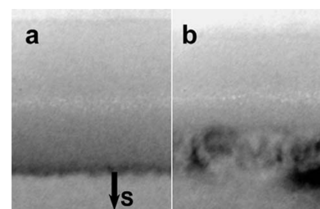

FIG. 3. ⟨110⟩ cross-sectional bright-field TEM images captured from video during a hot-stage experiment at a temperature of 620 °C, kinematical diffraction conditions, and underfocus. (a) Frame taken before the anneal showing the *a*-*c* interface. (b) Frame taken during the anneal showing that the SPEG takes place first at the interface that is closer to the surface. "S" indicates the direction of the surface.

the same time. SPEG takes place first at the interface that is closer to the surface and it is only when approximately half the amorphous layer has recrystallized that SPEG begins at the deeper-lying interface. This can be seen in Fig. 3 where two frames from an *in situ* experiment are presented. Diffraction contrast in the recrystallized region renders it generally visible. Note that in this experiment, the temperature of the specimen was increased until recrystallization was observed to begin at 620 °C. The specimen was then held at this temperature until recrystallization was complete. The SPEG has begun at the shallower interface at this temperature as evidenced by the band of darker contrast. Previous experiments on SPEG of buried amorphous layers (on bulk specimens) have indicated that regrowth occurs initially at the deeper-lying *a*-*c* interface[20] and, indeed, the position of the peak in the bubble distribution following recrystallization [Fig. 2(a)] also serves as an indication that SPEG also occurred first at the deeper-lying interface in bulk specimens. The reversal of this trend in the cross-sectional TEM foils can possibly be attributed to stress relief in the thin sections that is not possible in bulk specimens.

Figures 4(a)–4(c) are images captured from the video recording of an *in situ* annealing experiment, in which the specimen was tilted into an orientation that favored Bragg

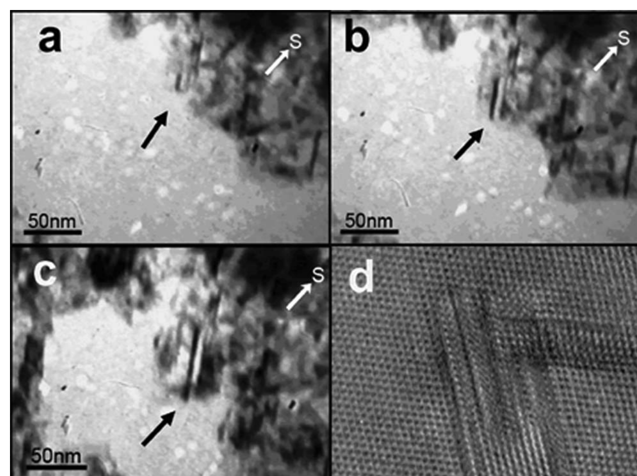

FIG. 4. ⟨110⟩ cross-sectional TEM images. (a), (b) and (c) bright-field images captured from video during a hot-stage experiment at a temperature of 620 °C, kinematical diffraction conditions and underfocus. Frames taken 70 s apart. Frame rate is 25 f/s. Black arrow indicates growing MTL. White arrow (S) indicates direction of surface. (d) High-resolution image of part of a MTL. Width of panel corresponds to 20 nm.

Downloaded 10 Nov 2008 to 194.167.47.253. Redistribution subject to ASCE license or copyright; see http://jap.aip.org/jap/copyright.jsp

diffraction by the MTLs so that these are visible as dark linear features. By slightly underfocusing the objective lens the cavities are also made visible in these images. The three images show the formation and growth of a MTL in a region approximately 50 nm distant from the nearest bubble. Such formation and growth were observed in a number of cases and, contrary to previous conclusions from *ex situ* experiments, MTLs were never observed to nucleate on a cavity. It is important to note, however, that in similar experiments carried out on identical buried amorphous layers not containing cavities, MTL formation did not occur, indicating that some aspect of the He implantation and/or cavity formation must be responsible for the MTL nucleation. Figure 4(d) shows a high-resolution phase contrast image of a part of a MTL, which includes the region where nucleation occurred (SPEG occurred from approximately the top left-hand corner of the image). The MTL has apparently nucleated in a very small volume of crystal and increased in width as it grew. Many MTLs viewed at high-resolution exhibited this trait.

The only defects that are observed in the *a*-Si following implantation of helium are the cavities (consisting of vacancies and helium); however, when an identical implantation is carried out in crystalline silicon, a dense distribution of interstitial clusters is also observed by means of diffraction contrast; a contrast mechanism that is not available in *a*-Si. During annealing, these clusters evolve into extended defects that include {311} rodlike and ribbonlike defects or dislocation loops.[21]

Although implantation of silicon with any ion gives rise to interstitial-type defects, it is important to note a significant difference between implantation with He (and other cavity-forming species) and implantation with other types of ions, such as the Li used to form the amorphous layer. In the latter case, the vast majority of interstitials formed in the cascades recombine with vacancies leaving only a relatively small number of residual defects described for self-ions, for instance, by the so-called "+1 model"). In the case of implantation with He, however, each He atom effectively "pins" a number of vacancies in the bubbles so that they cannot recombine with interstitials. For instance, using an equation of state for high-pressure helium according to Mills *et al.*,[22] it can be shown that there will be approximately 2.25 vacancies associated with each helium atom in an equilibrium bubble in Si with a radius of 5 nm (equilibrium pressure approximately 4 kbar). However, for an underpressurized bubble of this radius (or indeed a large equilibrium bubble) at a pressure of 400 bar, say, the number of vacancies per helium would be much higher (of order of ten). The formation of bubbles thus results in a significantly larger number of surviving interstitials than implantation with other species. This is clearly evident in the case of room temperature He implantation of crystalline silicon, where a high density of noncrystallographic interstitial-type defects is formed concomitantly with small bubbles.

Roorda *et al.*[23] carried out a detailed study of amorphous silicon irradiated with various ions, including He, and proposed that the defect structure in ion-irradiated amorphous silicon could be expected to be similar to that in ion-beam damaged crystalline silicon, i.e., that *a*-Si may also contain interstitial clusters (but note that these would give rise to little or no contrast variation in *a*-Si). These calorimetric measurements also indicated that only a small degree of relaxation of the defect structure in *a*-Si takes place at 400 °C and an extrapolation of these results to higher temperatures would indicate that interstitial defects may still exist in *a*-Si at the recrystallization temperature of 550–650 °C.

Of course, the definition of an interstitial atom or interstitial cluster in *a*-Si is less clear than in *c*-Si, and they may be considered merely to be localized variations in density. Such a description may provide an interpretation of the irregular nature of the cavities in *a*-Si shown in Fig. 1(a), as local variations in density would result in local variations in elastic moduli, which may give rise to localized variation in the curvature of the cavities.

In the present work, the MTLs are observed to nucleate at the moving a/c interface in regions where there are no bubbles. However, as indicated above, the calculated damage distribution resulting from the He irradiation has been superimposed on the dark-field image in Fig. 2(b), and indicates that the MTLs occur in regions of the *a*-Si where the radiation damage from the He implantation is above a threshold value. As the damage in this region is expected to be interstitial in nature (with the corresponding vacancies "pinned" in the cavities), this would appear to provide strong circumstantial evidence for the interstitials being responsible for MTL nucleation in our experiments.

To test this hypothesis, molecular dynamics (MD) simulations of the SPEG process have been performed, silicon being described with the EDIP potential (Environment-Dependent Interatomic Potential).[24,25] This interatomic potential has previously been used for investigating SPEG in silicon and its use resulted in good agreement with experiments.[26] Although it has been recently suggested that this potential might not correctly reproduce SPEG due to the melting of *a*-Si in the course of the process,[27] this point has not been confirmed by our own test calculations. We have performed the SPEG simulations in a way similar to Bernstein *et al.*,[26] i.e., our initial systems, with dimensions $5a_0$ (X=[100]), $5a_0$ (Y=[010]), and $10a_0$ (Z=[001]), were formed by joining a crystalline slab $5a_0 \times 5a_0 \times 4a_0$ with a disordered structure $5a_0 \times 5a_0 \times 6a_0$ along the Z direction. Periodic boundary conditions were applied only along X and Y, leaving two free surfaces and a single *a*-*c* interface. Several models of disordered structures were built, with a density increased by 5% and 10% compared to *c*-Si, in order to investigate whether the presence of defects would induce MTL formation. Initial samples, with the same density as *c*-Si, were prepared by slow quenching of liquid silicon and showed the characteristic features of *a*-Si. The first model was made by randomly introducing interstitials into the disordered structures, which were then relaxed (model I). In a second model, we randomly introduced small clusters containing ten interstitials and relaxed the structures (model II). Model III is similar to model II, except that several annealing and quench cycles were performed to optimize the relaxation of the interstitial clusters. Finally, a fourth model was obtained by quenching liquid silicon prepared with the desired density (model IV). For each model, six different samples

Downloaded 10 Nov 2008 to 194.167.47.253. Redistribution subject to ASCE license or copyright; see http://jap.aip.org/jap/copyright.jsp

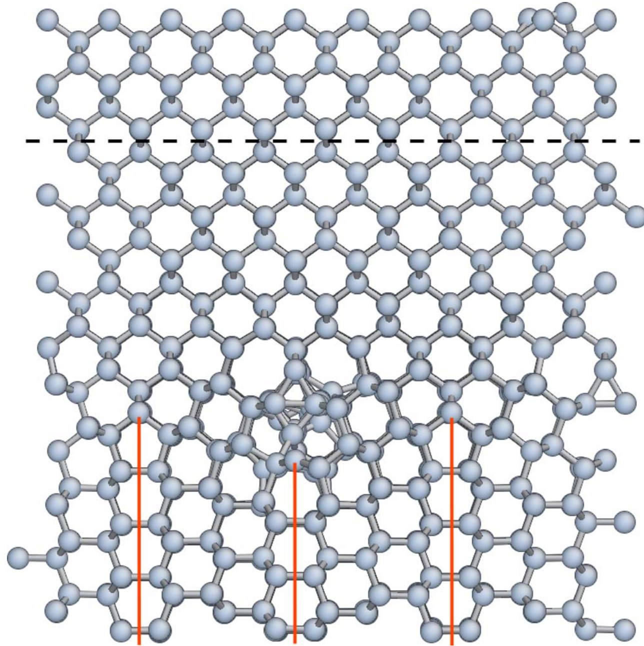

FIG. 5. (Color online) Ball-stick representation, projected onto (110), of a selected final configuration after SPEG (edges are not shown for clarity). Recrystallization occurred from top to bottom, starting from the initial *c*-*a* interface (dashed line), with the formation of a grain boundary and a change in growth direction from ⟨110⟩ to ⟨112⟩. Stacking faults, present in the ⟨112⟩ region, are also marked in the picture (full line).

were built, i.e., a total of 24 samples for a given density. SPEG simulations were then carried out using MD runs of 10 ns, i.e., 10^7 time steps, and a constant temperature of 1100 K obtained by velocity rescaling, followed by a final relaxation.

We first of all describe the SPEG process for *a*-Si with the same density as *c*-Si. Almost all simulations led to a complete and perfect recrystallization of the disordered structure, except in one case where two stacking faults formed during the process. No attempts have been made to estimate the rate of the recrystallization since this is out of the scope of this paper. Considering now *a*-Si systems with a density increased by 5% or 10%, we found that many have recrystallized, with the extra interstitial atoms having migrated toward the surface. However, in several of them, either incomplete recrystallization or formation of stacking faults or grain boundaries is obtained. These events can be classified into three categories:

(i) complete recrystallization with the formation of one or several stacking faults,

(ii) stacking faults bordering a small disordered region, and

(iii) amorphous nuclei leading to the formation of a grain boundary, with a possible change in growth orientation and the presence of stacking faults. An example of this category is shown in Fig. 5.

Overall, we found that the occurrence of such events increases with the density of the disordered structure, the number of events for 10% being twice that for 5%. There are few differences among the different models; although it appears that there are slightly more events in the case of models I and IV than for models II and III. All these observations suggest that the probability of formation of structural defects increases with the concentration of interstitials in the initial amorphous material. It is likely that interstitials or clusters of interstitials form locally metastable structures, which then act as nuclei for defects that form on recrystallization or alternatively that they increase the migration barrier for silicon atoms in *a*-Si, thus hindering recrystallization.

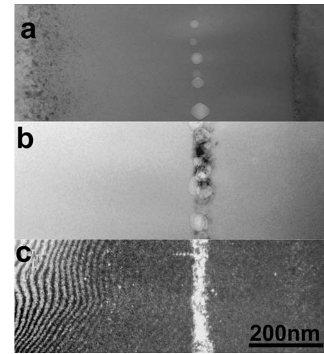

FIG. 6. ⟨110⟩ cross-sectional TEM image of a cavity layer created in *c*-Si using He implantation and a 1000 °C anneal, and a subsequent Li implantation to create a buried amorphous region. (a) Bright-field image, taken down zone, kinematical diffraction conditions, and underfocus (showing large cavities in the center of the buried *a*-Si layer). [(b) and (c)] TEM images after a recrystallizing anneal at 620 °C, where it can be seen that almost no MTLs have formed in this case. (b) Bright-field image using [111] two-beam conditions, kinematical diffraction conditions, and underfocus. (c) Corresponding dark-field TEM micrograph.

The formation of stacking faults or thin grain boundaries during SPEG simulations is associated with a change in growth orientation. MTLs are obtained during the process, as a perfect crystal slab bordered by two stacking faults with similar orientations. These calculations thus provide confirmatory evidence for the role that interstitials in the *a*-Si play in the formation of MTLs at the *a*-*c* interface.

In addition, to provide further support for this hypothesis, a cavity layer was created in *c*-Si using an identical He implantation to that used to create the cavity layer in the *a*-Si. The specimen was then annealed at high temperature (1000 °C) at which all interstitial-type defects in *c*-Si are known to be removed. The *c*-Si was then amorphized using the same Li implantation as previously. This anneal also resulted in a coarsening of the cavity distribution and a loss of helium from the specimen. The resulting morphology then consisted of large cavities in the center of the buried *a*-Si layer—but without the high density of interstitials created by the He implantation [Fig. 6(a)]. Note that although some interstitials will inevitably be introduced into the amorphous layer by means of the Li-induced amorphization step, as a consequence of the factors discussed above combined with the lower fluence, the concentration would be expected to be approximately a factor of 10 lower than that due to the He implantation.

Cross-sectional dark-field and bright-field images of this specimen following SPEG at 550–600 °C are shown in Figs. 6(b) and 6(c), where it can be seen that almost no MTLs have formed in this case apart from a very small density at the peak of the cavity distribution.

Downloaded 10 Nov 2008 to 194.167.47.253. Redistribution subject to ASCE license or copyright; see http://jap.aip.org/jap/copyright.jsp

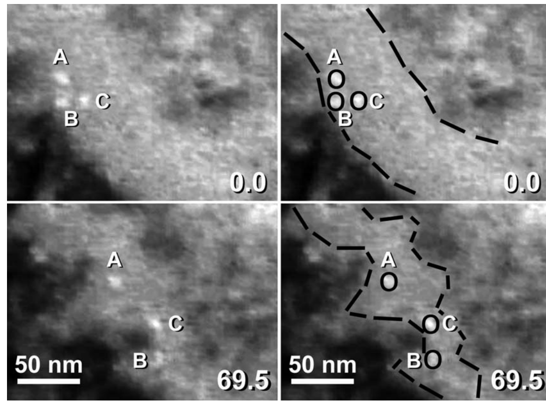

FIG. 7. ⟨110⟩ cross-sectional bright-field TEM images captured from video during a hot-stage experiment at a temperature of 620 °C, kinematical diffraction conditions, and underfocus. The recrystallized region can be identified by the presence of (dark) diffraction contrast. The two images in the left-hand column have been repeated in the right-hand column, but in this case, for clarity, both the approximate positions of the a/c interfaces (dashed line) and the positions of three bubbles (circles) have been delineated. The numbers on the two frames indicate time in seconds from an arbitrary starting time. Note that the region of the specimen shown in the two images is the same, but that both of the *a*-*c* interfaces has moved toward the bubbles. The three individual bubbles marked A, B, and C in the two frames can clearly be seen to have moved and to have remained within the amorphous material.

In summary, in He-implanted *a*-Si, MTLs form during (100) SPEG, with a distribution indicating a possible association with interstitial-type defects, and during *in situ* anneals are clearly seen to nucleate remote from the cavities. During SPEG of a similar *a*-Si layer containing cavities but approximately a factor of 10 fewer interstitial-type defects (i.e., where those resulting from the He implantation have been removed), almost no MTLs are observed to form. We propose, on the basis of these observations and MD simulations, that MTL formation is promoted by the presence of interstitial-type defects in the *a*-Si at the *a*-*c* interface.

B. Interaction of moving *a*-*c* interface with cavities

The results shown in Fig. 1 indicated that the cavity distribution had moved following SPEG, implying a possible interaction between the moving *a*-*c* interfaces and the cavities. If the cavities are in some way swept by the moving interface, it would open up the possibility of using this process as a means of producing narrow cavity distributions that could have applications in technologies such as the ion cut process and proximity gettering.

Once again, *in situ* annealing experiments have served to shed considerable light on this process, and the reader is referred to a videoclip of such an experiment[19] as the information conveyed by the moving images is difficult to reproduce merely using still frames. Figure 7 shows frames captured from an *in situ* experiment. Note that the images have been contrast enhanced to render the bubbles more clearly visible. In addition, the two images in the left-hand column have been repeated in the right-hand column, but in this case, for clarity, both the approximate positions of the a/c interfaces (dashed line) and the positions of three bubbles (circles) have been delineated. The numbers on the two frames indicate time in seconds from an arbitrary starting time. The frames are taken from annealing experiment in which the specimen temperature was approximately constant at 620(±10) °C over the period between the two observations. Note that the region of the specimen shown in the two images is the same but that both of the *a*-*c* interfaces have moved toward the bubbles. The three individual bubbles marked A, B, and C have been followed frame-by-frame in the videoclip and the figure serves to demonstrate that all three bubbles have moved and have remained within the amorphous material. (Note that the dark contrast results from diffraction effects within the recrystallized material.) This motion, and that of other bubbles, is unequivocal when the videoclip itself is viewed.[19] The bubbles can also be seen to be generally confined to the amorphous region. From a series of video frames at 5 s intervals, measurements of the projected two-dimensional (2D) movement of a small number of bubbles have been made, yielding, for bubbles with radii in the range from approximately 4 to 6 nm, projected velocities along their 2D projected trajectories of between 2.5 and 1.5 nm/s at a temperature of 620 °C.

Cavity mobility in Si almost certainly results from surface migration processes, whereby the migration of atoms at the cavity surface leads to a stochastic displacement of the center of mass of the cavity and gives rise to a Brownian motion, with smaller cavities moving more rapidly than larger ones. In *c*-Si, cavity mobility has been observed only at somewhat higher temperatures.[28,29] The observed bubble mobility at lower temperatures in *a*-Si implies that surface diffusion in *a*-Si has a lower activation energy than that on *c*-Si surfaces.

In a previous paper,[28] an expression has been derived for cavity velocity v_c along the projected path, observed from successive video frames recorded with a frame rate of $1/\Delta t$,

$$v_c = 2(\lambda/N)\sqrt{\frac{v_0[\exp(-E_s/kt)]}{\Delta t}}, \tag{1}$$

where λ is the atomic jump distance, N is the number of vacancies in the cavity, E_s is the activation energy for surface diffusion, ν_0 is the jump attempt rate, T is temperature, and k is Boltzmann's constant.

Using the range of values for bubble radii and velocity cited above, and assuming a value for ν_0 of 10^{13} s^{-1}, this expression yields a value for the activation energy for surface diffusion on amorphous silicon in the range of 0.35–0.45 eV. For crystalline silicon, measurements have been made of diffusion processes on *c*-Si surfaces; for instance, Swartzentruber and Schacht[30] indicated an activation barrier of 1.3 eV for surface diffusion that involves the removal of atoms from steps. This value is higher than those measured for Si ad-dimers or Si monomers on the Si (001), which are 0.94 and 0.7 eV, respectively.[31]

For diffusion on *a*-Si surfaces, however, the literature reports values only for hydrogenated *a*-Si. For example, Bray and Parsons[32] reported an activation energy of 0.2 eV, which is consistent with a hydrogen-mediated precursor diffusion process. Recent calculations using MD simulation yield an average diffusion barrier of approximately 0.16 eV for SiH_3 diffusion on *a*-Si:H growth surface.[33] For a clean *a*-Si surface, it is to be expected that the energy for the

Downloaded 10 Nov 2008 to 194.167.47.253. Redistribution subject to ASCE license or copyright; see http://jap.aip.org/jap/copyright.jsp

creation and migration of a surface adatom would be lower than that for a perfect planar crystalline surface, the inevitable irregular nature of the *a*-Si surface perhaps yields migration barriers similar to those at steps or ledges in *c*-Si.[34] The current measurements indicate that surface migration on *a*-Si may take place with an activation energy of as low as 0.35–0.45 eV; however, this would appear to be an anomalously low value, raising the question as to whether the implanted Li used to create the *a*-Si could play a role in modifying surface diffusion activation energies. Work is in progress to measure bubble mobilities in *a*-Si created by Si implantation, with a view to obtain more precise information of surface diffusion in *a*-Si.

We, therefore, conclude tentatively that the range of values for the activation energy for surface diffusion on *a*-Si deduced from expression (1) are higher than that for *a*-Si:H, but lower than values measured on *c*-Si. The bubble mobility clearly indicates that, in our experiments, the surface mobility on *a*-Si is greater than that on *c*-Si. Finally, returning to Fig. 1 and the observation of much larger bubbles following He implantation into *a*-Si compared to implantation of *c*-Si under identical conditions: the activation energy for surface migration that we have deduced leads to the conclusion that small bubbles in *a*-Si will be mobile at room temperature (and thus during the He implantation), and so will grow by thermally induced motion and coalescence as well as by any radiation-induced processes. For instance, a bubble of 4 nm radius would be expected to migrate at about 0.1 $\mathrm{nm\,s^{-1}}$ at RT. The observation of larger bubbles in the as-implanted *a*-Si is, thus, also consistent with a lower activation energy for surface diffusion than for *c*-Si.

IV. CONCLUSIONS

A study has been carried out of the solid phase epitaxial regrowth of buried amorphous layers in silicon in which helium-filled cavities have been formed by ion implantation. As with previous work, the presence of the cavities was observed to result in the formation of a high density of MTLs in the recrystallized material. Contrary to the conclusions of the earlier work, however, we have shown that the microtwins are not generally nucleated on the cavity surfaces but, rather, result from the presence of interstitials at the amorphous-crystalline interface, the presence of interstitials giving rise to the stacking error that causes a microtwin to nucleate.

A second important observation is that, during SPEG, cavities are confined to the amorphous side of the moving interface resulting in a net movement of the cavity distribution. This is due to a significantly greater cavity mobility in amorphous silicon than in the crystalline phase. As cavity mobility arises from surface diffusivity, we conclude that surface diffusivity in the amorphous phase is significantly higher than that in the crystalline.

ACKNOWLEDGMENTS

We acknowledge the support of the Alliance/Egide program (French Ministère des Affaires Etrangères and the British Council) and also of the French-Brazilian CAPES-COFECUB program. M.F.B. thanks Pr. P.F.P. Fichtner for fruitful discussions. A.S.G. acknowledges support from the Science and Technology Department of the French Embassy in London and S.E.D. acknowledges support from the University of Poitiers for extended visits to the Laboratoire de Physique des Matériaux in Poitiers.

[1]S. E. Donnelly, R. C. Birtcher, C. Templier, and V. Vishnyakov, Phys. Rev. B **52**, 3970 (1995).
[2]R. C. Birtcher, S. E. Donnelly, M. Song, K. Furuya, and K. Mitsuishi, Phys. Rev. Lett. **83**, 1617 (1999).
[3]S. E. Donnelly, R. C. Birtcher, C. W. Allen, I. Morrison, K. Furuya, M. Song, K. Mitsuishi, and U. Dahmen, Science **296**, 507 (2002).
[4]*Fundamentals Aspects of Inert Gases in Solids*, NATO Advanced Studies Institute, Series B: Physics, edited by S. E. Donnelly and J. H. Evans (Plenum, New York, 1991), Vol. 279.
[5]R. E. Hurley, S. Suder, and H. S. Gamble, Vacuum **76**, 291 (2004).
[6]G. A. Petersen, S. M. Myers, and D. M. Follstaedt, Nucl. Instrum. Methods Phys. Res. B **127–128**, 301 (1997).
[7]S. M. Myers, G. A. Petersen, D. M. Follstaedt, T. J. Headley, J. R. Michael, and C. H. Seager, Nucl. Instrum. Methods Phys. Res. B **120**, 43 (1996).
[8]S. M. Myers and D. M. Follstaedt, J. Appl. Phys. **86**, 3048 (1999).
[9]D. A. Brett, G. de M. Azevedo, D. J. Llewellyn, and M. C. Ridgway, Appl. Phys. Lett. **83**, 946 (2003).
[10]V. M. Vishnyakov, S. E. Donnelly, and G. Carter, J. Appl. Phys. **94**, 238 (2003).
[11]E. Oliviero, S. Peripolli, L. Amaral, P. F. P. Fichtner, M. F. Beaufort, J. F. Barbot, and S. E. Donnelly, J. Appl. Phys. **100**, 043505 (2006).
[12]A. S. Gandy, S. E. Donnelly, M. F. Beaufort, E. Oliviero, and P. F. P. Fitchner, Nucl. Instrum. Methods Phys. Res. B **257**, 177 (2007).
[13]E. Oliviero, P. F. P. Fichtner, A. Gandy, S. E. Donnelly, M. F. Beaufort, and J. F. Barbot (unpublished).
[14]J. F. Ziegler, J. P. Biersack, and U. Littmark, *The Stopping and Range of Ions in Solids* (Pergamon, New York, 1985), http://www.srim.org/.
[15]L. Pelaz, L. A. Marqués, and J. Barbolla, J. Appl. Phys. **96**, 5947 (2004).
[16]G. Nabert and H. U. Habermeier, Appl. Phys. Lett. **58**, 1074 (1991).
[17]P. Revesz, M. Wittmer, J. Roth, and J. W. Mayer, J. Appl. Phys. **49**, 5199 (1978).
[18]M. Wittmer, J. Roth, P. Revesz, and J. W. Mayer, J. Appl. Phys. **49**, 5207 (1978).
[19]S. E. Donnelly, Videoclips available at http://www.imr.salford.ac.uk/fm/sed/media.php.
[20]M. K. El-Ghor, O. W. Holland, C. W. White, and S. J. Pennycook, J. Mater. Res. (to be published).
[21]M. F. Beaufort, S. E. Donnelly, S. Rousselet, M. L. David, and J. F. Barbot, Nucl. Instrum. Methods Phys. Res. B **242**, 565 (2006).
[22]R. L. Mills, D. H. Lievenberg, and J. C. Bronson, Phys. Rev. B **21**, 5137 (1980).
[23]S. Roorda, W. C. Sinke, J. M. Poate, D. C. Jacobson, S. Dierker, B. S. Dennis, D. J. Eaglesham, F. Spaepen, and P. Fuoss, Phys. Rev. B **44**, 3702 (1991).
[24]M. Z. Bazant, E. Kaxiras, and J. F. Justo, Phys. Rev. B **56**, 8542 (1997).
[25]J. F. Justo, M. Z. Bazant, E. Kaxiras, V. V. Bulatov, and S. Yip, Phys. Rev. B **58**, 2539 (1998).
[26]N. Bernstein, M. J. Aziz, and E. Kaxiras, Phys. Rev. B **61**, 6696 (2000).
[27]C. Krzeminski, Q. Brulin, V. Cuny, E. Lecat, E. Lampin, and F. Cleri, J. Appl. Phys. **101**, 123506 (2007).
[28]S. E. Donnelly, V. M. Vishnyakov, R. C. Birtcher, and G. Carter, Nucl. Instrum. Methods Phys. Res. B **175-177**, 132 (2001).
[29]S. E. Donnelly, in *Ion Beam Science: Solved and Unsolved Problems*, Danish Academy of Sciences and Letters, Copenhagen, edited by P. Sigmund, Matematisk-fysiske Meddelelser **52**, 329 (2006).
[30]B. S. Swartzentruber and M. Schacht, Surf. Sci. **322**, 83 (1995).
[31]B. S. Swartzentruber, Phys. Rev. Lett. **76**, 459 (1996).
[32]K. R. Bray and G. N. Parsons, Phys. Rev. B **65**, 035311 (2001).
[33]M. S. Valipa, T. Bakos, and D. Maroudas, Phys. Rev. B **74**, 205324 (2006).
[34]Q. M. Zhang, C. Roland, P. Boguslawski, and J. Bernholc, Phys. Rev. B **75**, 000101 (1995).

Downloaded 10 Nov 2008 to 194.167.47.253. Redistribution subject to ASCE license or copyright; see http://jap.aip.org/jap/copyright.jsp